Conference on Modelling Fluid Flow (CMFF'22)
The 18th International Conference on Fluid Flow Technologies
Budapest, Hungary, August 30 -September 2, 2022

LOCAL FLOW RESOLUTION WITH THE BLOCKED-OFF METHOD IN DEM-CFD: GASEOUS FUEL JET DISPERSION AND COMBUSTION IN A PARTICLE ASSEMBLY

Enric ILLANA[1,2], Max BRÖMMER[2], Siegmar WIRTZ[2] and Viktor SCHERER[2]

[1] Corresponding Author. Tel.: +49 234 / 32-25340. E-mail: illana@leat.rub.de
[2] Institute of Energy Plant Technology, Ruhr-University Bochum, Universitätsstraße 150, 44780 Bochum, Germany

ABSTRACT

DEM-CFD simulation of reacting flows inside large-scale granular assemblies remains a challenging task. Resolving the flow field within the voids is required to obtain correct conversion rates but due to the computational resources required, this high resolution cannot be employed on the device-scale. In the current work, a combined approach is employed: the so-called blocked-off method is used to resolve the voids between particles within a prescribed refinement region, while the volume-averaged method is applied to the rest of the domain because of its low computational effort. This approach is firstly tested in a case where nitrogen is injected into an air cross-flow. A good agreement with oxygen concentration measurements is obtained when applying the blocked-off method to the whole domain and locally, whereas the volume-averaged method under-predicts the local oxygen concentration since jet dispersion is too low. The latter is also observed in a second case where methane is injected in cross-flow into an air stream with subsequent reaction of the methane. As a result, the locally resolved approach predicts significantly larger reaction rates associated with higher maximum temperatures as well a larger spread of the area with high temperatures than the volume-averaged method.

Keywords: Dispersion, Bulk, Blocked-Off, AVM, DEM-CFD

NOMENCLATURE

A	$[m^2]$	area
d	$[m]$	characteristic face size
Nu	[-]	Nusselt number
Pr	[-]	Prandtl number
Re	[-]	Reynolds number
S	[-]	source term
T	$[K]$	temperature
U	$[m/s]$	velocity
Y	[-]	mass fraction
$\dot{Q}$	$[J/s]$	rate of heat transferred
h	$[W/(m^2\ K)]$	heat transfer coefficient
k_r	$[10^{16}\ /s]$	reaction rate
$\dot{m}$	$[mg/s]$	mass flow
p	$[Pa]$	pressure
w	[-]	weighting factor
ϕ	[-]	solution variable
κ	$[W/(m\ K)]$	thermal conductivity
H	$[m]$	height
W	$[m]$	width
L	$[m]$	length
n	[-]	number of CVs

Subscripts and Superscripts

CV	control volume
N	neighbour
face	triangle of the polyhedron surface
fluid	interpolated from the fluid phase
air	at the air inlet boundary
CH4	at the methane inlet boundary
part	related to the particles
L	lance
B	bottom
AVM	averaged-volume method
BO	blocked-off method

1. INTRODUCTION

A gaseous fluid passing the bulk as a heating or cooling agent or as a system-specific reactant adds a second phase to the system. Its general flow direction may be counter-, parallel- or cross-flow with respect to the solid movement, depending on the system and the product properties pursued. Large forces accompanying the movement of the bulk, high temperatures and a generally poor accessibility from outside of the reactor render the measurement of temperature or concentration profiles within those technical systems nearly impossible. Thus, detailed investigation of the

processes within the bulk and in vicinity of the fluid injection must resort to numerical simulations of the tightly coupled two-phase problem. In principle, coupled DEM-CFD simulations provide the framework for a comprehensive numerical description of the transport and reaction processes. For a more detailed overview on the status on DEM-CFD simulations of reactive particle systems, we refer to [1-4].

Considering the large number of actual particles in many industrial reactors, the numerical description is typically constrained to the so-called unresolved methods, where the bulk particles are represented as a porosity field within the volume-averaged Navier-Stokes equations of the fluid phase (acronym AVM for Averaged Volume Method [1]). Although this approach is applicable to industrial-scale shaft kilns [5], it lacks a detailed description of the flow field within the voids between the particles, thus cannot directly determine effects related to the unresolved scales.

To be specific, in lime shaft kilns the gaseous fuel enters through nozzles at the tip of lances extending into the descending bulk material and releases heat and combustion products in vicinity of the nozzle outlet where the moving lime particles partially block the passage. Discretizing the voids and their temporal development locally in front of the nozzles can solve this issue but must be embedded in a larger, device-spanning AVM solution to capture air preheating and stone cooling in a reasonable fashion. As a consequence, a combined method exploiting both, resolved voids in vicinity of the inlets and the cost-effective AVM in the remaining domain is pursued.

2. PRIMARY OBJECTIVES AND MODEL DESCRIPTION

The long-term scientific objective of the current work is the numerical description of a configuration, where a secondary combustive gas stream is injected orthogonally into a confined flow, only that the flow domain is additionally obstructed by a moving, heat-exchanging and reacting solid bulk. Mixing of the injected fuel flow with the preheated cooling air occurs within the void space between the particles. In comparison to an unconstrained conventional cross-flow situation, length scales of mixing are severely limited and local residence times are short, both requiring much higher local resolution than on the overall device scale.

As a first step towards this goal, AVM-based momentum, heat and mass transfer, tightly coupled with a locally void-resolving method are employed with OpenFOAM (fireFoam, v2012) and an in-house DEM code in order to evaluate the feasibility of the blocked-off method (BO) for this purpose.

2.1. DEM and particle flow

Assuming spherical particles with constant properties instead of employing the actual shape of the limestone objects allows to simplify the geometric complexity of the current study. In case of spheres, a conventional linear spring-dashpot model, which connects a virtual overlap of the spheres with a repulsion force, is employed as the contact force model in the current Discrete Element (DEM) code.

The code used in this study is an ongoing development within the collaborative research centre Bulk-Reaction, which is funded by the German Research foundation [6]. In this code, position vectors (centres of gravity) and quaternions (orientations) are the solid's transport variables while detailed information (if required) on the highly resolved particle shape (triangulated surface) is stored separately in so-called prototypes. This hierarchical structure, besides other advantages, avoids the continuous position update of all corner-points of the objects and restricts it to the required points. At the same time this allows a fast identification of the CVs to be blocked such that the remaining CVs correctly represent a discretisation of the voids between the particles.

2.2. AVM for device-spanning transport

The AVM considers any particle in the flow domain, respectively the discrete elements as their conceptual representations, as a Lagrangian object interacting with one or several CVs. In the current implementation, each element determines the dependence of its properties and source terms on averaged fluid properties ϕ from the closest CVs as

$$\phi_{elem} = \sum w_{CV} \phi_{CV} \quad (1)$$

$$\sum w_{CV} = 1 \quad (2)$$

with volume-related weights depending on a Gaussian kernel function. The source terms determined for the particles must be distributed in the same way to the respective CVs. A similar smoothing method is described in [7], where the volume of a particle is distributed outwards from the cell containing the particle's centre of gravity so that the porosity value of all cells is above a threshold. These processes of weighting, averaging and spatial smoothing are particularly important as they determine energy and mass conservation as well as the required computational effort. If the particles are distinctively smaller than the CVs, the mapping between the particle sources and the CVs is unambiguous, while the assignment of fluid properties to spatial positions within the CV still requires spatial interpolation, since linear profiles of state variables within the CVs are a core assumption of finite volume methods. Therefore, AVM is best suited for CVs larger or of comparable size than the

particles and where a low flow resolution is sufficient since flow gradients are small. The computational effort of this method is low because of the little amount of particle-CV interactions.

2.3. Blocked-off method for locally resolved void space

In vicinity of the inlets, the local mesh resolution must be high enough to sufficiently resolve the voids between particles. A straightforward choice would be a tetrahedral body-conformal discretisation resolving the space available for the fluid as employed by [8] to investigate the effect of different approximations of the particle contact representation in a static assembly of spheres. If moving particles have to be considered, where the voids deform and thus change volume and shape over time, a continuous re-meshing and value interpolation would be required which is tedious and time consuming. A simpler, and especially with respect to computational efficiency cheaper method, is the BO method, initially proposed by Patankar [9]. It enforces artificial boundary conditions within a static mesh and appropriately blocks the control volumes (CVs) partially or fully obstructed by the boundaries of steady or moving objects. The respective CVs are dynamically identified and excluded from the solution by linearizing the source terms in the discretised transport equations of a CFD solver.

In finite volume methods, this requires the solution of a system of equations resulting from the balance of fluxes across the surfaces of control volumes. These balances lead to discretized transport equations for a solution variable ϕ which, in their generic form, are:

$$a_c \phi_c + \sum_{N_{c,c}} a_N \phi_N = S_\phi \tag{3}$$

where *N* refers to the control volumes adjacent to the CVs while a_c and a_N are matrix coefficients containing the information related to the mesh and discretisation scheme. S_ϕ, the source term, combines all terms resulting from the temporal change of ϕ. Non-linear terms on the left hand side of Eq. (3) as well as the boundary values are moved to the right hand side of the equation, but are not shown here for brevity. For stability reasons, the general source term S_ϕ is implemented in a linearized form:

$$S_\phi = S_c - S_p \phi \tag{4}$$

This allows to move the product $S_p \phi$ to the left hand side of Eq. (3), where it enters the matrix on the diagonal, thus increasing diagonal dominance.

$$(a_c + S_p)\, \phi_c + \sum_{N_{c,c}} a_N \phi_N = S_c \tag{5}$$

The field values S_c and S_p exist for every CV and are readily accessible outside the underlying solution procedure. Therefore, they can be employed to prescribe the value of a solution variable ϕ in any control volume of a given mesh without changes to the matrix itself or the associated coefficients. Thus, they provide an efficient interface to reflect boundaries of moving discrete objects within the domain.

At the position of any object larger than the local mesh size (for simplicity a homogenous Cartesian mesh is employed here), its presence within the flow domain can be represented by a cluster of core-CVs and surface-CVs. The solution variable ϕ is forced to the value of S_c by setting S_p to a large number (e.g. 1e20). For fluid flows, as momentum is undefined in the core-CVs, $S_c = 0$ essentially blocks momentum transport, while the pressure based continuity equation automatically enforces mass conservation in the remaining CVs which form the voids. Further details on the implementation of this approach are given in [10] and explained for radiative heat transfer in [11].

2.4. Heat transfer model

In any reacting system, the heat transfer is essential as it often controls the reaction processes via temperature. Considered here are the heat released in the gas phase due to fuel combustion, convective enthalpy transport within the gas phase, convective transport within the solid phase and the mutual enthalpy exchange between the two phases. To keep things simple in this first conceptual test, outer boundaries (except inflow and outflow) are considered adiabatic and heating of the particles is suppressed by a constant particle temperature of 850 °C, corresponding to the calcination temperature of lime. Thus, the plausible assumption is that all heat transferred to the particles is consumed for calcination. Note that radiative heat transfer among particles has been neglected in this preliminary study. Considering non-moving particles corresponds to the situation of solid residence times being much larger than the gas residence time. This is a reasonable simplification which is valid for many shaft kiln applications.

Convective heat exchange between particles and the surrounding fluid flow is calculated on the DEM side by applying the Newton's law of cooling to the total surface of the particle:

$$\dot{Q}_{face} = A_{face}\, h\, \left(T_{fluid} - T_{face}\right) \tag{6}$$

where h is the heat transfer coefficient. As the sphere's surface is represented by a triangulated immersed mesh, it is computed locally from the

Nusselt number correlation for flat plates under laminar conditions:

$$Nu = \frac{h\,d}{\kappa_{fluid}} = 0.664\,\sqrt{Re_{face}}\sqrt[3]{Pr_{face}} \qquad (7)$$

The characteristic length L of the transfer is computed from the face area. In the case that a particle is outside the blocked-off region, h and T_{fluid} are equal for all the faces. The overall heat transferred is equally distributed as an energy source to the CVs that are in contact with the particle. If the particle is however inside the BO region, the $\dot{Q}_{face}$ is distributed to the closest CVs that are not blocked.

2.5. Combustion model

A laminar combustion regime is assumed in this work. The following single-step irreversible reaction is considered for modelling the chemical process:

$$CH_4 + 2\,O_2 \rightarrow CO_2 + 2\,H_2O \qquad (8)$$

All species mass fractions are transported except Y_{N2}, which is calculated so that the sum of all mass fractions equals unity. The reaction rate k_r is defined by [12]:

$$k_r = 5.2\,e^{-\frac{14906}{T}} \qquad (9)$$

The fluid thermophysical and transport properties are calculated from the resulting composition and temperature fields.

3. INVESTIGATED TEST CASES

Two different test cases have been considered in the current feasibility study. The first one is based on an experimental study from literature, investigating the injection of a nitrogen flow through a lance into a static regular simple cubic (sc) packing of spheres vertically passed by air [8] and the resulting mixing profiles. The second test case comprises the injection of fuel into a similar generic section of a lime shaft kiln, where it mixes and reacts with the air passing through the assembly. Strictly laminar flow is assumed and the particles are considered non-moving for simplicity.

3.1. Verifying mixing in isothermal cross-flow

The experimental setup has been taken from literature [8] and it is sketched in Figure 1. Particle diameter is 52 mm and the immersion depth of the lance into the bed is 156 mm. The experiments were performed by introducing nitrogen through the lance into the vertically passing laminar air flow. The concentration of oxygen in the passing airflow is obtained as a measure of the mixing. Further details on flow parameters and experimental conditions can be found in the original paper [8].

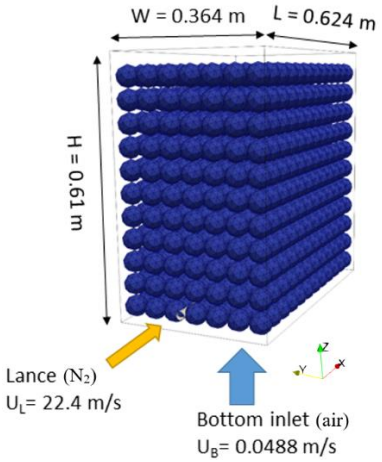

Figure 1. Arrangement of spheres (sc) and location of the lance.

When simulating this arrangement, a major disadvantage of conventional body-conforming tetrahedral meshes resolving the voids space in the whole domain would be the large number of small control volumes required and the challenge to generate a mesh with good properties for an arbitrary arrangement of spheres. Additionally, an adaption to the large difference in length scales (wide inflow with small velocities at the bottom versus comparably high velocity at the tip of the lance) requires considerable effort in this approach.

As an alternative, a structured Cartesian mesh with three different cell size levels, as sketched in the middle of Figure 2, is employed in the current work. The AVM method is applied to the red zone of the domain where the spheres have a similar size as the CVs, while BO is used within the turquoise refinement area and allows to better resolve the flow in vicinity of the lance tip. Furthermore, one pure AVM simulation as well as a fully resolved BO simulation were conducted.

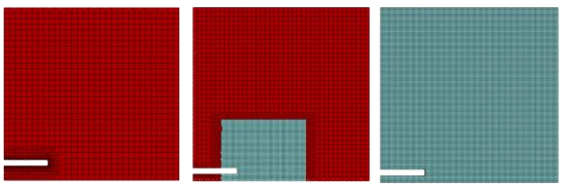

Figure 2. Vertical cut through the mesh at the position of the injection lance for pure AVM (left), locally refined AVM/BO (middle) and fully refined BO approach (right). For the AVM/BO approach, particles are resolved at the region with the lowest cell size level.

The associated meshes are depicted in Figure 2 and the respective numbers of CVs are $n_{AVM} = 29{,}466$ cells, $n_{AVM/BO} = 250{,}688$ cells and $n_{\mathrm{BO}} = 2{,}175{,}408$ cells. Taking computational time with the AVM as the reference, the AVM/BO approach requires 8 times more and the fully refined case 48 times more for the same simulated time.

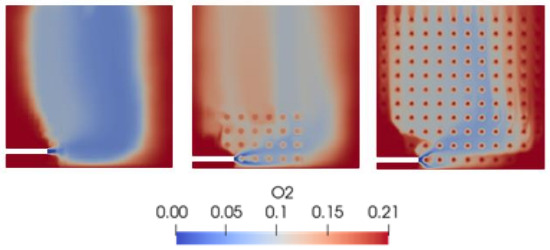

Figure 3. Oxygen mass fraction at the vertical cut for AVM (left), BO (right) and combined AVM-BO methods (middle)

The oxygen mass fraction distribution at the same vertical cut is plotted in Figure 3 for the three approaches considered. In general, the AVM simulation shows a higher oxygen mass fraction in comparison to the two other configurations, indicating that the mixing in crosswise direction of the lance is under-predicted.

Note that since a uniform air composition has been imposed at the start time, and equal to the cross-flow composition, the blocked cells keep in this case an oxygen mass fraction of 0.21. Thus, small dots (representing a part of the particles) are visible within the resolved regions.

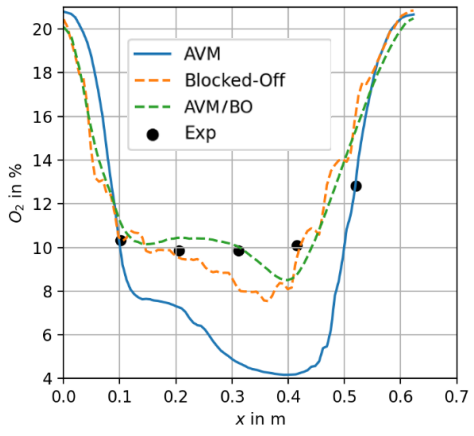

Figure 4. Oxygen mass fraction profiles at a line located 0.468 *m* above the lance

In Figure 4, the mass fraction profiles of oxygen obtained from the different approaches at a height of 0.468 m above the lance axis, i.e. a line along the x direction in the vertical cut, are compared with the measurements from [8]. It can be observed that the use of the AVM method results in low O_2 concentrations due to the reduced mixing of the nitrogen flow with the vertical airflow, while the BO approach is able to reproduce the oxygen concentration level obtained in the measurements. A similar agreement, exhibiting an even higher resolved structure, is observed if the whole domain has the same resolution as the region near the injection. The combined AVM/BO approach in particular, delivers a reasonably smooth and comparable solution for a lower computational cost.

3.2. Combustion of methane injected into a generic shaft kiln section

The previous example has confirmed that the combined AVM/BO approach is able to capture the mixing of a flow introduced through a lance into a crossflow passing through a bulk. The aim of this test case is to determine the influence of the mixing resolution on the combustion process, in terms of flame location and temperature distribution, as occurring in the heating section of lime shaft kilns.

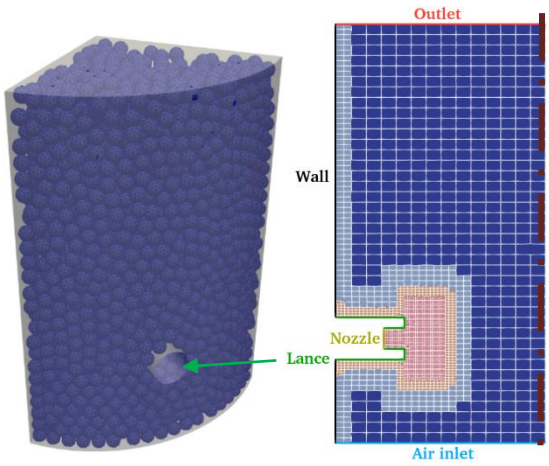

Figure 5. Vertical cut of the mesh at the lance position (left) and particle distribution (right) of the generic lime shaft.

Figure 5 sketches the simulated geometry, which shows the particle assembly as well as a cut of the CFD mesh at the injector, and the relevant dimensions are included in Table 1.

Table 1. Geometric measures of the generic shaft in meters

Radius	1
Height	2
Nozzle diameter	0.1
Lance diameter	0.2
Lance immersion length	0.3
Largest cell size	0.05
Particle diameter	0.08

Table 2. Boundary conditions imposed for both the AVM and locally resolved methods

p_{outlet}	101325
$\dot{m}_{CH4}$	0.028
$\dot{m}_{air}$	0.46
T_{CH4}	300
T_{air}	300
T_{part}	850

For this test case, in order to have a clear comparison between the methods when a reacting flow is computed, the same mesh is used. To do so, since the cells are significantly smaller than the particle size, a uniform porosity level of 0.4 is applied in the regions where AVM is applied. For the simulation with the combined AVM/BO approach, particles are resolved when they lie within the second refinement level (i.e. orange and red cells in Fig. 5, where the cell size is 0.0125 or lower) and a porosity value of 1 is set. The conditions imposed at the boundaries and to the particles can be found in Table 2. The imposed mass flows lead to a cross flow velocity of 0.5 m/s and a jet velocity of 5.5 m/s. The overall equivalence ratio is 1.05.

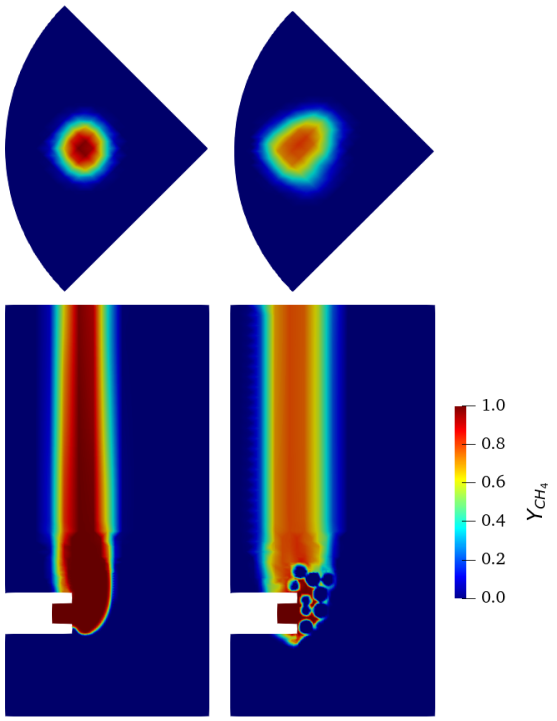

Figure 6. Y_{CH4} distribution at the outlet (top) and middle plane (bottom), AVM (left) and locally resolved (right) AVM/BO method.

The comparison of the methane distribution is performed in Figure 6. It clearly shows that, as stated in the previous test case, the AVM solution presents a reduced amount of mixing and dispersion when compared to the AVM/BO solution. Additionally, since local combustion regime is in this case diffusion-dominated, due to the locally rich conditions at the reaction zone, the amount of burned CH_4 is also highly influenced by the flow mixing. Simulation results indicates that with the AVM only 4.24% of the injected fuel is actually converted to CO_2, while the 10.88% of methane has reacted when using the local refinement by AVM/BO. The latter has in turn a large impact on the temperature field, displayed in Figure 7, where the maximum temperature as well as the area with high temperatures are larger with the combined AVM/BO method. The spatial average at the outlet boundary results in a mean exit temperature of 384.8 K for the AVM and 534.6 K for the locally resolved AVM/BO method.

Regarding the flame shape, a smaller flame surface and thinner flame brush are obtained with the AVM. The stabilization point also differs between both simulations since with the AVM/BO approach it is located below the lance, further upstream of the cross flow.

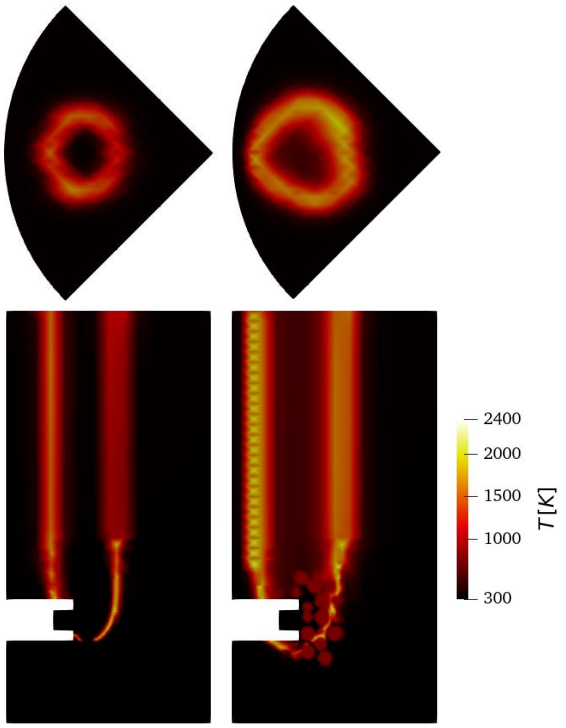

Figure 7. Temperature distribution with the AVM (left) and locally resolved AVM/BO (right) method at the outlet (top) and middle plane (bottom).

4. SUMMARY

The Averaged Volume Method (AVM) is widely used in DEM-CFD approaches to simulate large-scale systems, due to the low computational effort required. It is however limited to meshes with large cell sizes, larger

than the particle size, which does not allow for local flow resolution in the voids among particles. A reduced jet dispersion is a consequence. To properly capture the mixing and reaction processes of gaseous flows and, hence, the associated particle reaction in a particle assembly it is crucial to resolve the voids between particles in critical areas, i.e. in areas with high gradients. For such configurations, the combination of the AVM with the blocked-off (BO) approach presented in this work has shown good agreement with oxygen concentrations measured experimentally in a jet (nitrogen)-crossflow (air) arrangement for a packed bed with spherical particles. The importance of the local flow resolution using the AVM/BO approach is stressed in a reacting flow simulation of a similar jet (methane)-crossflow (air) arrangement: the amount of methane burnt is doubled in the combined AVM/BO solution and thus the averaged exit temperature is around 150 degrees higher.

Although the computing time for the AVM/BO approach is higher (for the current case 8 times) such investment in computing time might be needed to reliably predict lime quality as the quality (reactivity) of the lime depends on material temperature (and residence time).

Note that the method presented can also be applied to turbulent conditions and with moving particles of irregular shape.

ACKNOWLEDGEMENTS

This work has been funded by the Deutsche Forschungsgemeinschaft (DFG, German Research Foundation) – Project-ID 422037413 – TRR 287.

Gefördert durch die Deutsche Forschungsgemeinschaft (DFG) – Projektnummer 422037413 – TRR 287.

REFERENCES

[1] Golshan, S., Sotudeh-Gharebagh, R., Zarghami, R., Mostoufi, N., Blais, B., and Kuipers, J., 2020, "Review and implementation of CFD-DEM applied to chemical process systems", *Chemical Engineering Science*, 221, 115646.

[2] V. Scherer, S. Wirtz, B. Krause, and F. Wissing, 2017, "Simulation of reacting moving granular material in furnaces and boilers an overview on the capabilities of the discrete element method," *Energy Procedia*, 120, 41–61.

[3] B. Peters *et al.*, 2019, "XDEM multi-physics and multi-scale simulation technology: Review of DEM–CFD coupling, methodology and engineering applications," *Particuology*, 44, 176–193.

[4] Z. Peng, E. Doroodchi, and B. Moghtaderi, 2020, "Heat transfer modelling in Discrete Element Method (DEM)-based simulation of thermal processes: Theory and model development," *Prog. Energy Combust. Sci.*, 79, 100847.

[5] Krause, B., Liedmann, B., Wiese, J., Bucher, P., Wirtz, S., Piringer, H., and Scherer, V., 2017, "3D-DEM-CFD simulation of heat and mass transfer, gas combustion and calcination in an intermittent operating lime shaft kiln", *International Journal of Thermal Sciences*, 117, 121-135.

[6] "Bulk Reaction", https://bulk-reaction.de (accessed Jan. 05, 2022).

[7] Spijker, C., Pollhammer, W. R., and Raupenstrauch, H., 2020, "Coupled Computational Fluid Dynamics and Discrete Element Method modelling of shaft furnace, including nitrogen emissions", *12th European Conference on Industrial Furnaces and Boilers*, Portugal.

[8] Alkhalaf, A., Refaey, H. A., Al-durobi, N., and Specht, E., 2018, "Influence of contact point treatment on the cross flow mixing in a simple cubic packed bed: CFD simulation and experimental validation", *Granular Matter*, 20, 22.

[9] Patankar, S., 1980, "Numerical heat transfer and fluid flow", *CRC Press*.

[10] Buss, F., Wirtz, S., and Scherer, V., 2020, "Simulation of a reacting agitated bed of straw pellets by a resolved coupled DEM/CFD method using a blocked-off approach", *International Journal of Thermal Sciences*, 152, 106332.

[11] Jaeger, B., Schlag, M., Scherer, V., Wirtz, S., and Schiemann, M., 2021, "Radiative heat transfer with a blocked-off approach for application in the discrete element method", *Powder Technology*, 392, 558-569.

[12] reactingFoam tutorial, www.openfoam.com (accessed Mar. 10, 2022).